POLITECNICO DI TORINO
Repository ISTITUZIONALE

Evaluation of the Wheeler-Jonas parameters for biogas trace compounds removal with activated carbons

Availability:
This version is available at: 11583/2648244 since: 2016-09-12T16:03:17Z

Terms of use:

This article is made available under terms and conditions as specified in the corresponding bibliographic description in the repository

(Article begins on next page)

02 May 2024

Evaluation of the Wheeler-Jonas parameters for biogas trace compounds removal with activated carbons

Davide Papurello[a,b], Luca Tomasi[b], Silvia Silvestri[b], Massimo Santarelli[a]

[a] Department of Energy (DENERG), Politecnico di Torino, Corso Duca degli Abruzzi, 24, 10129,

Turin, Italy.

[b] Fondazione Edmund Mach, Biomass and renewable energy Unit, Via E. Mach, 1, 38010, San

Michele a/A, Italy.

*Corresponding author. Tel.:+393402351692. Email address: davide.papurello@polito.it

Abstract

A practical and feasible solution to reduce the global impacts from fossil fuels, is represented by the locally distributed micro-cogeneration systems, with high temperature solid oxide fuel cells fed by biogenous fuel coupled in an energy distributed system. One of the main drawback for SOFCs fed by biogas, is the low tolerability towards certain fuel impurities, mostly sulfur, chlorine and siloxane compounds. The possibility to predict the breakthrough time of a gas cleaning section with a high precision level is mandatory. The reaction kinetic equation, called the Wheeler-Jonas equation, is adopted to estimate the breakthrough times of filters against organic vapors. In this work, the Wheeler-Jonas equation is adopted to investigate and to estimate the breakthrough time, the adsorption capacity and the overall adsorption rate capacity for two different commercial activated carbons, varying the operating temperature, the pollutant concentration (single and multiple effect) and the relative humidity value. Results showed how relative humidity content, above RH 20% in the biogas affects inversely the removal performance for both sorbents. Carbox sample, below RH 20% shows better results due to its metals content and microstructure. Here, relative humidity promotes the best condition to remove organic vapors from the biogas stream. Multiple contaminant condition (H_2S+HCl), for both sorbent materials, decreases the removal performance (t_b). This decreasing, for Carbox, ranges from a minimum of 44% to a maximum of 50% for H_2S and 70% for HCl, with wet and dry condition, respectively.

Keywords: Adsorption, VOCs removal, Biogas, Solid Oxide Fuel Cell (SOFC), Carbon, Wheeler-Jonas equation.

Nomenclature:

- A_{tot}, total water that can be adsorbed (g_{water}/g_{coal}),
- B, structural carbon constant (K^{-2}),
- C_0, initial concentration (g/cm^3),
- C_s, contaminant concentration at the saturation pressure (g/cm^3),
- C_w, water concentration in the gas stream (g/cm^3),
- C_x, breakthrough concentration (g/cm^3),
- D, unit of dipole moment (debye),
- d_b, bed depth (cm),
- d_l, liquid density of the organic vapor (g/cm^3),
- d_p, carbon particle average diameter (cm),
- H_2S, hydrogen sulfide,
- HCl, hydrogen chloride,
- k_v, overall adsorption rate coefficient (min^{-1}),
- $k_{v,wet}$, adsorption global coefficient with humid condition (min^{-1}),
- m and k, Langmuir constant,
- MW, molecular weight (g/mol),
- p_1^0, p_2^0 model parameter,
- PDMS, polydimethylsiloxane membrane,
- PID, Proportional Integrative and Derivative controller,
- P_S, saturation pressure of the pollutant (mbar),
- P_w, saturation pressure of the water (mbar),
- Q, volumetric flow rate (cm^3/min),
- RH, Relative Humidity,
- SOFC, Solid Oxide Fuel Cell,
- T, operating temperature (K),
- t_b, breakthrough time (min),
- TPV, total pore volume,
- v_l, linear velocity through the bed (cm/s),
- VOCs, Volatile Organic Compounds,
- W, sorbent weight (g),
- W_0, micropore volume (cm^3/g_{coal}),
- W_e, equilibrium adsorption capacity ($g_{pollutant}/g_{coal}$),
- $W_{e,1-2}$, equilibrium adsorption coefficient of the component 1 or 2 ($g_{pollutant}/g_{coal}$),
- $W_{e,tot}$, equilibrium adsorption capacity of the binary mixture ($g_{pollutant}/g_{coal}$),
- W_{pre}, volume occupied by the pre-adsorbed water from the carbon (cm^3/g_{coal}),
- y_1, molar fraction of the component,
- ΔW_{gas}, volume occupied from the gas flow (cm^3/g_{coal}),
- ΔW_S, volume of water adsorbed and replaced from the pollutant (cm^3/g_{coal}),
- β, organic vapor coefficient,

- ρ_b, bulk density of the carbon bed (g/cm^3).

1. Introduction

Nowadays the exploitation of some fossil fuels such as diesel or gasoline fuel, natural gas and coal, satisfy the majority of the growing world energy demand. Due to the rapid population growth coupled to the industrial increasing requirements, the emissions from fossil fuels are destined to run out relatively quickly [1]. In addition, their global impacts are extremely harmful, such as the greenhouse effect, the hole in the ozone layer, acid rains and generalized environment pollution. In order to reduce or to narrow this problem, the renewable fuels employment in energy generation systems turns out to be fundamental. A practical and feasible solution to reduce the global impacts from fossil fuels, is represented by the locally distributed micro-cogeneration systems, with high temperature solid oxide fuel cells fed by biogenous fuel coupled in an energy distributed system [2,3]. These systems couple the high fuel conversion values of SOFCs, due to the electrochemical reactions instead of fuel combustion [4] and their remarkable fuel flexibility [5]. Biogas, from a biomass source is a viable alternative to fossil fuels in terms of energy generation performance and pollutant emissions [6]. This fuel is appropriate to be used in SOFC systems as reported in previous literature works [7–10]. Biogas is produced from organic matter digestion with methane and carbon dioxide as principal gas mixture elements. Next to these main constituents, a wide and variable range of trace compounds are contained in biogas [11]. One of the main drawback for SOFCs fed by biogas, is the low tolerability towards certain fuel impurities, mostly sulfur, chlorine and siloxane compounds that may decrease cell efficiency and degrade the fuel cell [12–17]. In order to achieve the biogas quality requirements for SOFC applications there are numerous techniques available which can be classified as biological, physical and chemical processes [18]. Biological processes are commonly used to reduce the pollutant emissions contained in the biogas. These treatments have significant economic advantages over other pollution control technologies. Biofiltration is a process by which contaminated gases pass through the biofilter and pollutants are transported into the biofilm, where they are utilized by microbes as a carbon source and energy source [19,20]. It is a process adopted to roughing the starting pollutant concentration from

thousands of ppm(v) to hundreds of ppm(v). Physicochemical processes can be classified as absorption (caustic washing), reactive (chemical oxidation) and adsorption techniques (iron and metal adsorbents, activated carbons), and they are appropriate only with low gas flow rates and low H_2S concentrations. Adsorption is the only technique which can reduce the concentration of contaminants to the stringent extent of fuel cell's specifications [21].

VOCs removal from activated carbon adsorption represents a valid and economic solution [22], even if some studies suggest alternative solutions [23]. For instance, Yuan et al., (2007) [24] reports that the surface of sludge derived adsorbents can be used for the desulfurization of digester gas. The removal capacity is comparable with catalytic activated carbons [24]. The main properties of activated carbon filters for the effective removal of VOCS are high porosity, high superficial area ($1500 \ m^2g^{-1}$), high volume, pore distribution [25] and treatment with metal ions. Physisorption and chemisorption are the two underlying physical phenomena of adsorption. The first one deploys weak Van der Walls forces whereas the second one involves the stronger covalent and ionic bonds. Van der Walls forces require polar or polarizable compounds. Typically, compounds with no dipole moment (0 D) are classified as non-polar, and else as polar, see table 1.

Compound	Dipole moment (Debye)	Reference
Hydrogen sulfide	0.95	[26]
Methanethiol	1.52	[26]
Dimetylsulfide	1.58	[26]
Propanethiol	1.55	[27]
Butanethiol	1.54	[27]
Chloroethane	6.7	[26]
2-Butanone	2.76	[26]
Toluene	1.3	[26]
Styrene	0.3	[26]
HF	1.82	[28]
HCl	1.08	[28]
HBr	0.82	[28]
HI	0.44	[28]

Table 1 – Dipole moment for VOCs of interest

Activated carbons are usually impregnated with metal ions because of the higher chemical affinity for organic compounds. Typical metals deployed are iron, copper, silver and chromium. These substances are able to promote the bond between carbon and polar molecules, such as sulfur, aromatic and carbonyl compounds [26,27,29,30]. In order to work with a SOFC generator fed by a biogenous fuel, the possibility to predict the breakthrough time with a high precision level is mandatory. The reaction kinetic equation, called the Wheeler-Jonas equation, is adopted to estimate the breakthrough times of filters against organic vapors [31–33]. Several research works were accomplished in order to investigate the predictability of different sorbent materials against different organic vapors [32–35]. Some organic vapors were investigated, for example: chlorine compounds, hydrocarbons (heptane, cyclohexane), ethanol and acetone. The Wheeler-Jonas equation is simple to be used for the comparison of model and experimental results, because it is based on solely measurable and readily available macroscopic parameters. This equation has been adopted to extrapolate single and multiple laboratory results by simply varying the independent variables of the equation, for example the weight of the carbon bed, the carbon material adopted, the initial concentration and the volumetric flow rate. Lack of the literature studies about the estimation of the breakthrough time for sulfur and chlorine compounds, principal compounds that affect SOFC performance, needs a specific investigation. In this work, the Wheeler-Jonas equation is adopted to investigate and to estimate the breakthrough time, the adsorption capacity and the overall adsorption rate capacity for two different commercial activated carbons, varying the operating temperature, the pollutant concentration (single and multiple effect) and the relative humidity value.

2. Material and methods

In this section are reported the characteristics of activated carbon materials used, the experimental set-up with the system description and the mathematical method used. The Wheeler-Jonas equation adopted is reported below and implemented with Matlab (Matlab R2012b, US):

$$t_b = \frac{W_e \cdot W}{Q \cdot C_0} - \frac{\rho_b \cdot W_e}{k_v \cdot C_0} \cdot \ln \frac{C_0 - C_x}{C_x} \ (Eq.1)$$

Where:

- W_e, equilibrium adsorption capacity ($g_{pollutant}/g_{coal}$),

- W, sorbent weight (g),

- Q, volumetric flow rate (cm^3/min),

- C_0, initial concentration (g/cm^3),

- C_x, breakthrough concentration (g/cm^3),

- ρ_b, bulk density of the carbon bed (g/cm^3),

- kv, overall adsorption rate coefficient (min^{-1}).

In the case of pure physisorption, especially for organic vapours, this equation needs two parameters of the carbon-adsorbate system to be calculated: the static adsorption capacity We and the overall adsorption rate coefficient, kv. The Dubinin–Radushkevich equation (Eq. 2) is adopted to calculate the adsorption capacity, We [36]:

$$W_e = W_0 \cdot d_l \cdot e^{\left[\frac{-B \cdot T^2}{\beta^2} \cdot \log^2 \frac{C_S}{C_0} \right]} (Eq.2)$$

Where:

- W_0, micropore volume (cm^3/g_{coal}),

- d_l, liquid density of the organic vapor (g/cm^3),

- B, structural carbon constant (K^{-2}),

- T, temperature (K),

- β, organic vapor coefficient,

- C_s, contaminant concentration at the saturation pressure (g/cm^3).

The estimation of the second parameter, the overall adsorption rate coefficient kv, is less straightforward. Initially some very crude estimation was developed, based on theoretical diffusion models. An alternative was the experimental determination of kv by means of a single breakthrough experiment [37]. Since then, several authors have proposed semi-empirical equations [38–42]. The most recent one has been put forward by Lodewyckx and Wood [42] (Eq. 3):

$$k_v = 800 \cdot \beta^{0.33} \cdot v_l^{0.75} \cdot d_p^{-1.5} \cdot \sqrt{\frac{W_e}{MW}} \ (Eq.3)$$

Where:

- kv, adsorption global coefficient (min^{-1}),

- v_l, linear velocity through the bed (cm/s),

- MW, molecular weight (g/mol),

- d_p, carbon particle average diameter (cm).

The physical and chemical properties are found in "The properties of gases and liquids" [43]. Two different commercial activated carbons, Norit (RST3, US) and Carbox (Airdep, Italy) were tested in the experimental setup reported in figure 1.
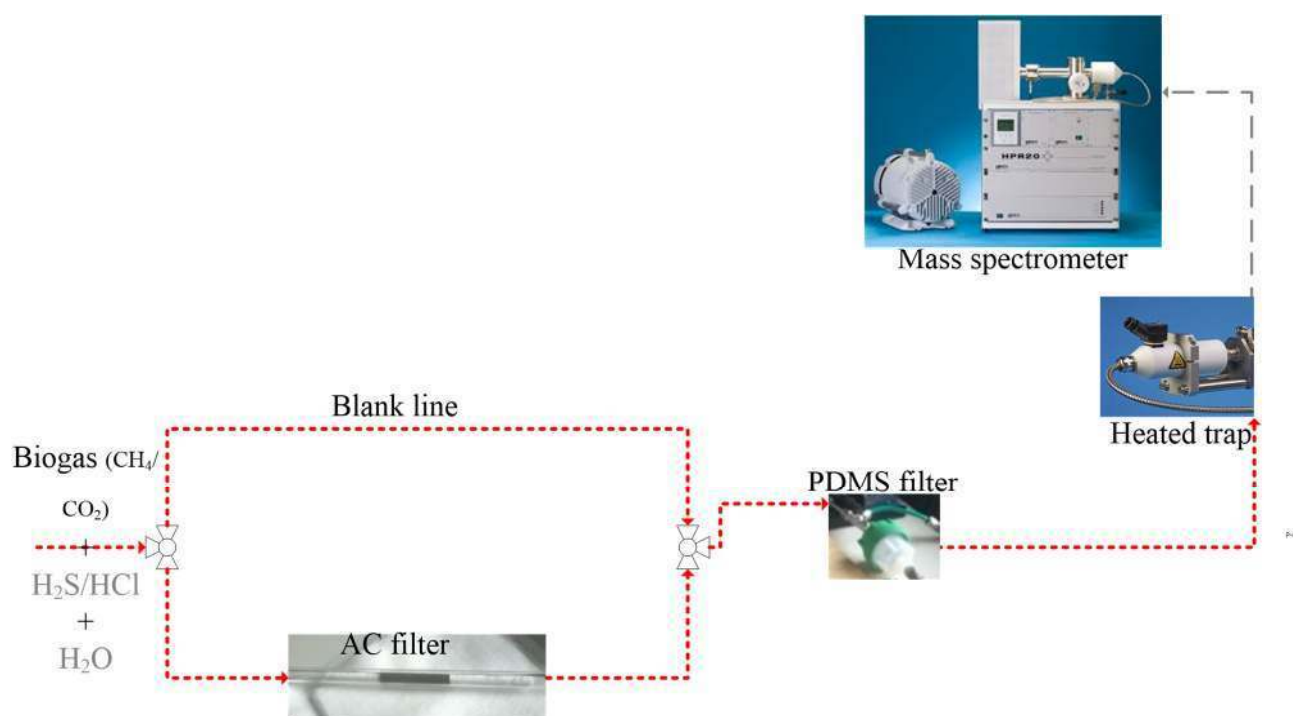
Figure 1 – Experimental set-up

Sample	Specific Surface Area (m²/g)	V total (cm³/g)	V microporous (cm³/g)
Airdep Carbox	1237	0.407	0.328
RST3	1117	0.447	0.300

Table 2 – Commercial activated carbons characteristics

Atomic %	Virgin		Tested	
Element	Carbox	RST3	Carbox	RST3
C	80.9	91.15	86.96	93.83
O	9.01	5.3	8.37	4.6
Mg	1.19	0.2	0.1	0.08
Al	1.98		0.68	
Si	1.4		1.03	
P	0.81			

S	0.11	0.57	0.27	0.72
Cl	0.33		0.63	
K	0.78	0.78	0.21	0.37
Ca	1.65	0.76	1.03	0.4
Mn	0.41			
Fe	1.43		0.72	
Zn		1.15		
Total:	100	100	100	100

Table 3 – Elements identified with SEM-EDS analysis in the Carbox and RST3 sample.

Characteristics of sorbent materials adopted are indicated in table 2 and in table 3. The activated carbons were characterized in terms of specific surface area, total volume and microporous volume, in addition it was analyzed the elemental material composition. Elemental composition measurements were performed by scanning electron microscopy (SEM) (FEI Inspect, Philips 525 M) coupled with EDS (SW9100 EDAX) analysis. To measure the specific surface area of the two sorbent materials, adsorption isotherms for N_2 at 77 K were determined using a Quantachrome Autosorb 1 (Boynton Beach, Florida, USA). Samples were outgassed at 423 K overnight prior to the adsorption measurements. The equipment allows measurement of relative pressure of 10−6 bar. Specific surface areas have been calculated by B.E.T. (Brunauer–Emmett–Teller) model in the relative pressure range 0.04–0.1 bar.

The sorbent materials were tested with simulated biogas ($CH_4/CO_2 = 1.5$), H_2S with a variable concentration (5-200 ppm(v)), HCl with a variable concentration (5-200 ppm(v)) and the demineralized water content 0-80%. The biogas mixture was inserted to the experimental set-up with mass flow controllers (Bronkhorst, The Netherlands) whereas the pollutants contained in cylinder gas are prepared from (Siad spa, Italy). The demineralized water was added to the main stream using a liquid mass flow controller and a controlled evaporator mixer (Bronkhorst, The Netherlands). Fig. 1 depicts the experimental set-up adopted; red color represents the heated lines at 40 °C with heater strings (isopad Thermocoax, Germany) controlled via a PID regulator (Horst, Germany). A PDMS (20 μm) membrane filter, to protect the mass spectrometer from the carbon particles, was inserted between the filter line and the heated trap before the capillary line of the

mass spectrometer adopted for the measurements HPR 20 (Hiden Ltd., UK). The sorbent materials were grounded up to 100-180 μm with a vibratory sieve shaker (Fritsch, Germany). The filter cartridges were prepared with Teflon tubes with around 0.12 g of sorbent material. The wet conditions were estimated using the same relation reported above (eq.1); it will change the micropore volume. This volume is estimated using the Polanyi model [37][44][45]:

$$W_{0,wet} = W_0 - W_{pre} - \Delta W_{gas} + \Delta W_S \; (Eq.4)$$

Where:

- W_0, micropore volume in dry condition (cm^3/g_{coal}),

- W_{pre}, volume occupied by the pre-adsorbed water from the carbon (cm^3/g_{coal}),

- ΔW_{gas}, volume occupied from the gas flow (cm^3/g_{coal}),

- ΔW_S, volume of water adsorbed and replaced from the pollutant (cm^3/g_{coal}).

Below are reported the relations necessary for the equation 4.

$$\Delta W_{gas} = \frac{\int_0^{tb} A_{tot} \cdot \left[1 - e\left(-\frac{0.00005 \cdot T \cdot v_L \cdot t}{d_g \cdot \sqrt{|A_{tot}|}} \right) \right] dt}{t_b} \; (Eq.5)$$

Where:

- A_{tot}, total water that can be adsorbed (g_{water}/g_{coal}),

- t_b, breakthrough time (min),

- T, operating temperature (°C),

- d_b, bed depth (cm),

- v_l, flow linear velocity (cm/s),

- ΔW_{gas}, volume occupied from the gas flow (cm^3/g_{coal}).

$$\Delta W_S = \left(W_{pre} + \Delta W_{gas}\right) \cdot \left[1 - \log\frac{C_w + C_0}{C_0} \cdot \log\frac{P_S + P_W}{P_W}\right] (Eq.6)$$

Where:

- C_0, contaminant concentration in the gas stream (ppm(v)),

- C_w, water concentration in the gas stream (ppm(v)),

- P_S, saturation pressure of the pollutant (mbar),

- P_w, saturation pressure of the water (mbar),

- W_{pre}, volume occupied by the pre-adsorbed water from the carbon (cm^3/g_{coal}),

- ΔW_{gas}, volume occupied from the gas flow (cm^3/g_{coal}),

- ΔW_S, volume of water adsorbed and replaced from the pollutant (cm^3/g_{coal}).

The adsorption global coefficient in wet condition was evaluated following the relation reported below:

$$k_{v,wet} = k_v \cdot \left(1 - \frac{A_{tot}}{TPV}\right)(Eq.7)$$

Where:

- A_{tot}, total water that can be adsorbed (g_{water}/g_{coal}),

- k_v, adsorption global coefficient (min^{-1}),

- $k_{v,wet}$, adsorption global coefficient with humid condition (min^{-1}),

- TPV, total pore volume.

The contemporary presence of H_2S and HCl was tested with dry (RH~0%) and wet conditions (RH~20%) to evaluate the effect on the Wheeler-Jonas parameters. The concentration for H_2S and HCl ranges from 9.6 pppm(v) and 12.7 ppm(v) at RH~0% up to 7.7 ppm(v) and 10.2 ppm(v) at RH~20%. Essentially the contemporary presence of more than one component affect the adsorption

capacity (We), it follows that also k_v and t_b are changed. The model adopted is based on the IAST model and on the Langmuir equation.

$$W_{e,tot} = \frac{m \cdot k \cdot C}{1 + k \cdot C} \ (Eq8)$$

Where:

- m and k, Langmuir constant,
- C_0, initial concentration of the pollutant (g/cm^3).

The amount of contaminant adsorbed is a binary mixture of HCl + H_2S, and it was modeled using the following relation:

$$\frac{1}{W_{e,tot}} = \frac{X_1}{W_{e1}} + \frac{1 - \left(\dfrac{p \cdot y_1}{p_1^{\,0}} \right)}{W_{e2}}$$

$$W_{e1} = W_{e,tot} \cdot \left(\frac{p \cdot y_1}{p_1^{\,0}} \right) \qquad (Eq.9)$$

$$W_{e2} = W_{e,tot} \cdot \left(1 - \left(\frac{p \cdot y_1}{p_1^{\,0}} \right) \right)$$

$$\frac{1 + k_1 \cdot p_1^{\,0}}{1 + k_2 \cdot p_2^{\,0}} = e \left(\frac{m_2}{m_1} \right) (Eq.10)$$

Where:

- m and k, Langmuir constant,
- $W_{e,1\text{-}2}$, equilibrium adsorption coefficient of the component 1 or 2 ($g_{pollutant}/g_{coal}$),
- $W_{e,tot}$, equilibrium adsorption capacity of the binary mixture ($g_{pollutant}/g_{coal}$),
- y_1, molar fraction of the component,
- p_1^0, p_2^0 model parameter.

3. Results and discussion

The Wheeler-Jonas equation was adopted to predict the breakthrough time varying several macroscopic conditions: operating temperature, inlet concentration in single and multiple configuration (H_2S and HCl) and relative humidity. In the sections reported below, the breakthrough times are modeled and compared to experimental values.

Breakthrough time and adsorption capacity affected by the pollutant concentration

Two different commercial activated carbons are tested; model and experimental results data for the breakthrough time varying the starting pollutant concentration for H_2S and HCl are reported in figure 2.
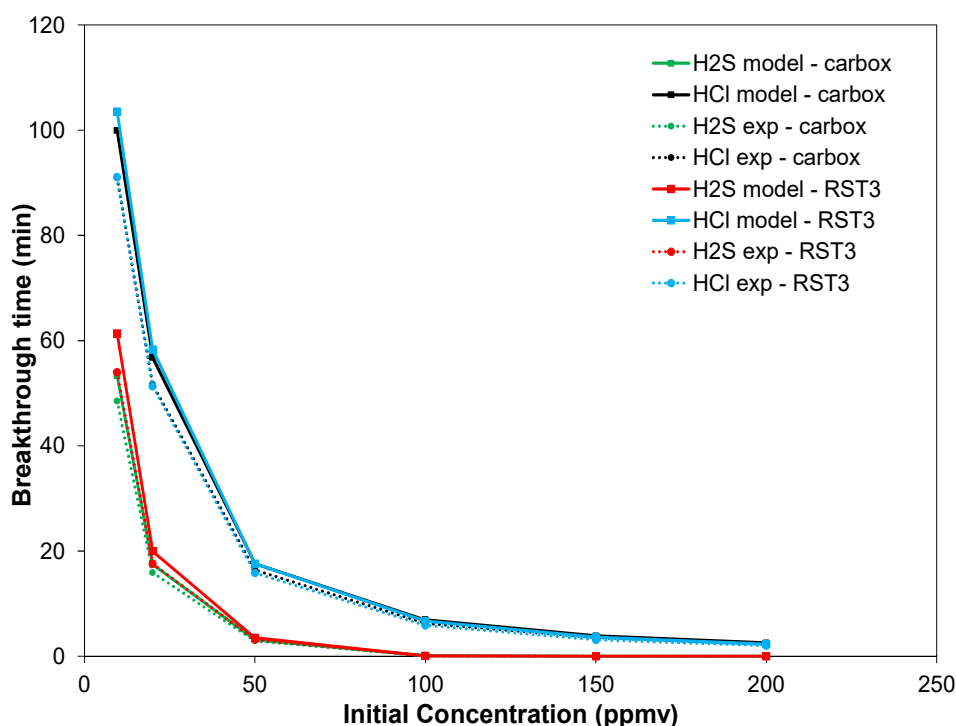

Figure 2 – Breakthrough time trend versus initial concentration of the pollutant

Breakthrough time values modeled with eq.1 are in agreement with experimental results, both in case of H_2S and HCl for the two different commercial activated carbon filters. The results confirm a marked decline in the t_b increasing the initial concentration of the contaminant, highlighting, on the contrary, an increase in the capacity of adsorption. In dry condition, RST3 carbon shows better results than Carbox sample. The biogas with a concentration of H_2S around 10 ppm(v), with RST3

shows a t_b around 60 min and 55 min, respectively in case of model and experimental condition. Considering the same biogas conditions, the Carbox sample shows a performance (t_b) around 54 min and 50 min, respectively in case of model and experimental condition. The biogas with a concentration of HCl around 10 ppm(v), with RST3, shows a t_b around 103 min and 91 min, respectively in case of model and experimental state. Considering the same biogas conditions, the Carbox sample shows a performance (t_b) around 99 min and 91 min, respectively in case of model and experimental status. Above 50 ppm(v) of concentration for H_2S the t_b is less than 5 min. The breakthrough time values, in case of HCl, are higher compared to H_2S for similar concentrations. This is due to the higher dipole moment of chlorine respect to sulfur which affect the removal capacity of the sorbent material. The Wheeler-Jonas equation, adopted as predictive model worked well with an overestimation of 8% at lower concentrations, while at higher concentration values there is an overestimation around 1%.
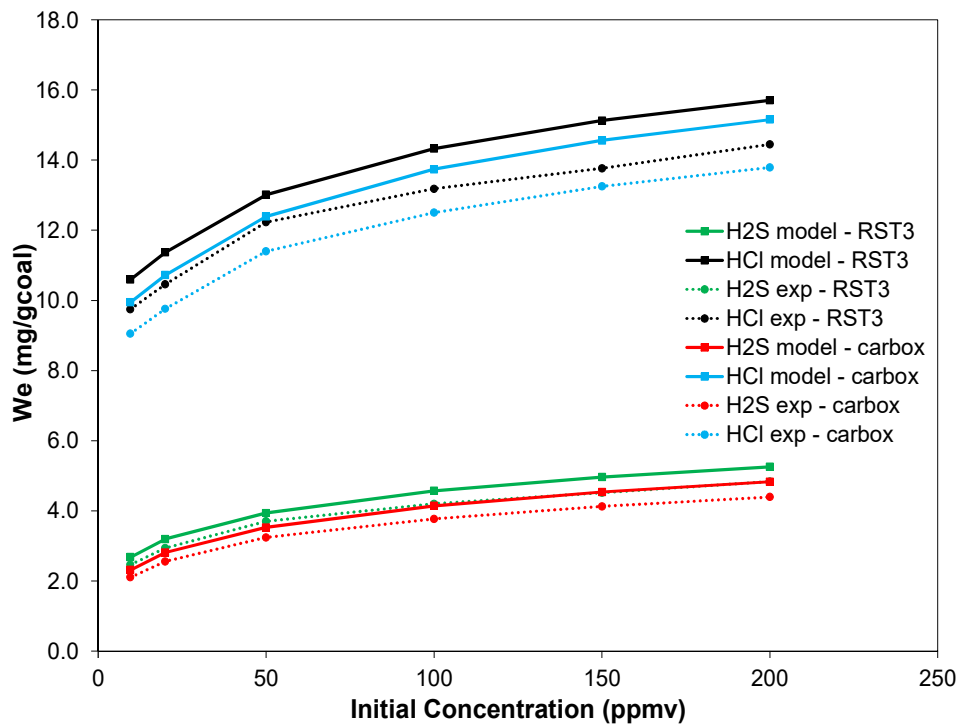
Figure 3 – Adsorption capacity trend versus initial concentration of the pollutant

Figure 3 depicts the adsorption capacity trend varying the starting pollutant concentration of H_2S and HCl. The biogas with a concentration of H_2S around 10 ppm(v), with Carbox sample shows an

adsorption capacity around 2.11 mg/g and 2.32 mg/g, respectively in case of experimental and model condition. Considering the same biogas conditions, the RST3 sample shows a performance (We) around 2.46 mg/g and 2.68 mg/g, respectively in case of experimental and model state.

Up to 200 ppm(v) of concentration for H_2S and HCl, the adsorption capacity (We) increases up to achieve the maximum value around 4.84 mg/g and 4.39 mg/g for RST3 and Carbox, in case of H_2S. The adsorption capacity for the HCl removal ranges from 14.45 mg/g and 13.79 mg/g for RST3 and Carbox respectively. The adsorption capacity values in case of HCl are higher compared to H_2S for similar concentrations.

Breakthrough time and adsorption capacity affected by the operating temperature

Breakthrough time values modeled with eq.1 are in agreement with experimental results, reported varying the operating temperature from 5 °C to 45 °C. Breakthrough time for HCl is in general higher respect to H_2S case, both for RST3 and Carbox. The two different commercial activated carbon filters show similar discrepancy from model and experimental values, from a maximum of 12%, at 5 °C, up to the minimum value of 6%, at 45 °C for Carbox sample. RST3 activated carbon shows lower discrepancy values compared to Carbox, from 9% at 5 °C up to 6% at 45 °C.
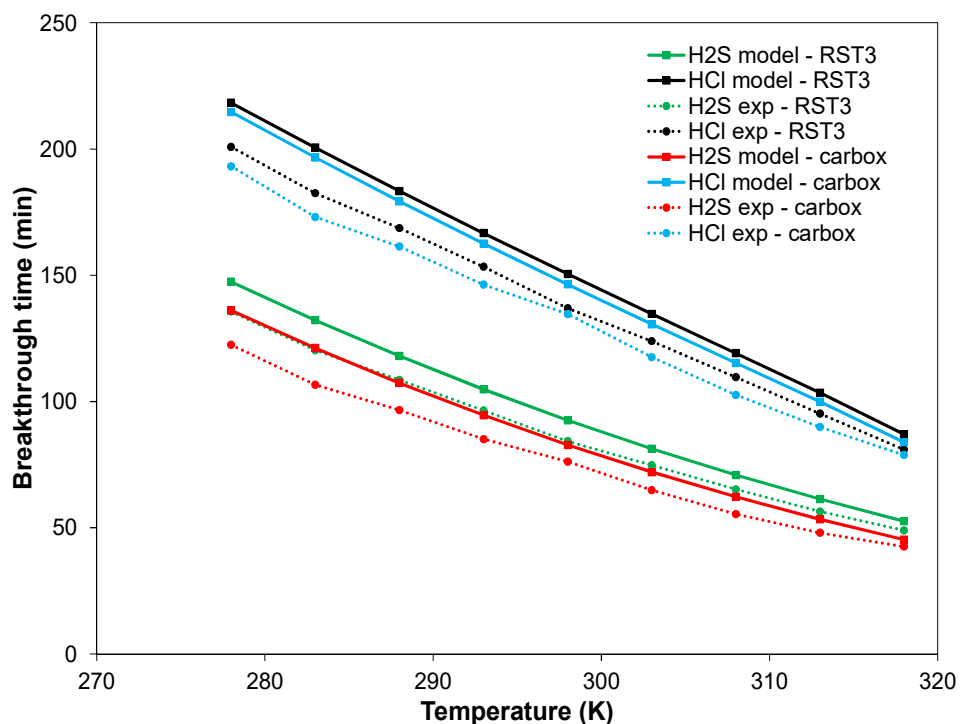
**Figure 4 – Breakthrough time trend versus operating temperature**

The results confirm a marked decline in the t_b increasing the operating temperature, from 5 °C up to 45 °C. The maximum breakthrough time value for RST3 at 5 °C is 135.6 min, for H_2S and 200.8 min for HCl with the minimum concentration around 9 ppm(v). The minimum breakthrough time value at 45 °C is 48.9 min for H_2S and 80.9 min for HCl. Considering the Carbox sample, the maximum t_b is 193 min and 122.4 min, respectively for HCl and H_2S at 5 °C. The minimum t_b value is 78.2 min and 42.5 min, respectively for HCl and H_2S at 45 °C. Increasing the operating temperature, the decreasing performance of the activated carbon is evidenced in figures 4 and 5. As the temperature rises, the vapor pressure of the adsorbate increases and hence raising the energy level of the H_2S and HCl molecules to overcome the Van der Waals attraction and migrate back to the bulk gas phase reducing the adsorption capacity and reducing the breakthrough time [46]. The breakthrough time and the adsorption capacity decreased slightly with the increasing of the operating temperature. This is due to the slightly exothermal process that will probably enhance chemisorption but has disadvantage on the physical adsorption [47,48]. Thus, an increase in the operating temperature caused lower values of the maximum capacity of the adsorbent.
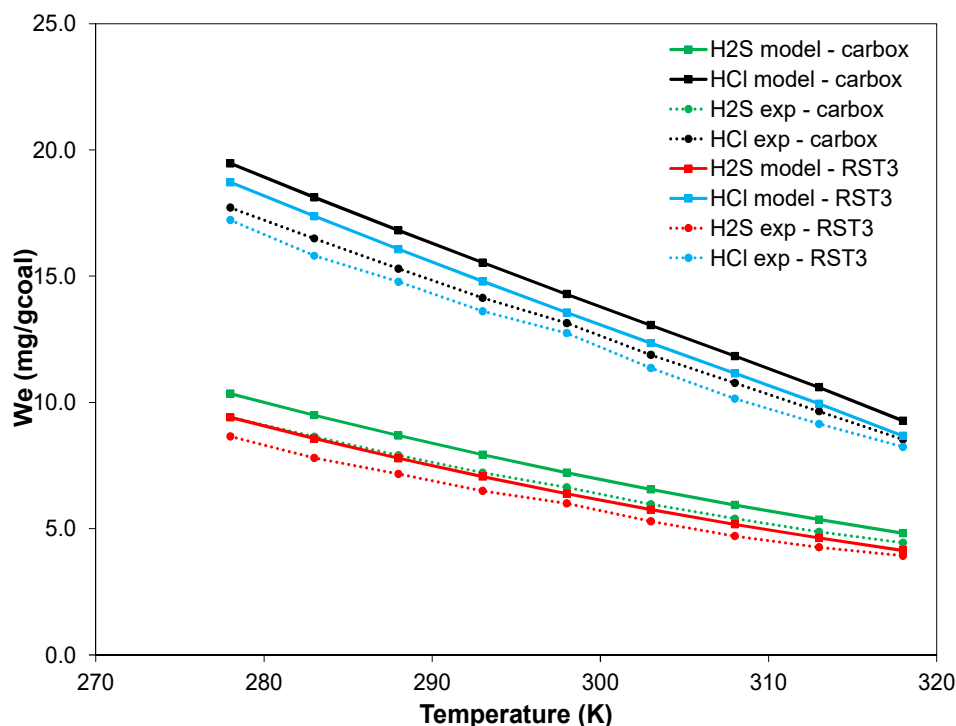
Figure 5 – Adsorption capacity trend versus operating temperature

Water humidity influence on the adsorption capacity

In figure 6 are reported the adsorption capacity of RST3 and Carbox for H_2S and HCl, varying the relative humidity at 30 °C. It is well known that water vapor, contained in the biogas, is pre-adsorbed on the carbon that will enter in competition with the organic vapor to be removed. This will usually result in a loss of adsorption capacity as well as a diminishing of the adsorption rate. In fact, when the relative humidity value is above 50% the adsorption capacity is zero. The maximum discrepancy between model and experimental values, for RST3, is 7.3% and 7.4% respectively for H_2S and HCl. Considering the Carbox sample the maximum discrepancy is 17.3% and 11.5% respectively for H_2S and HCl.
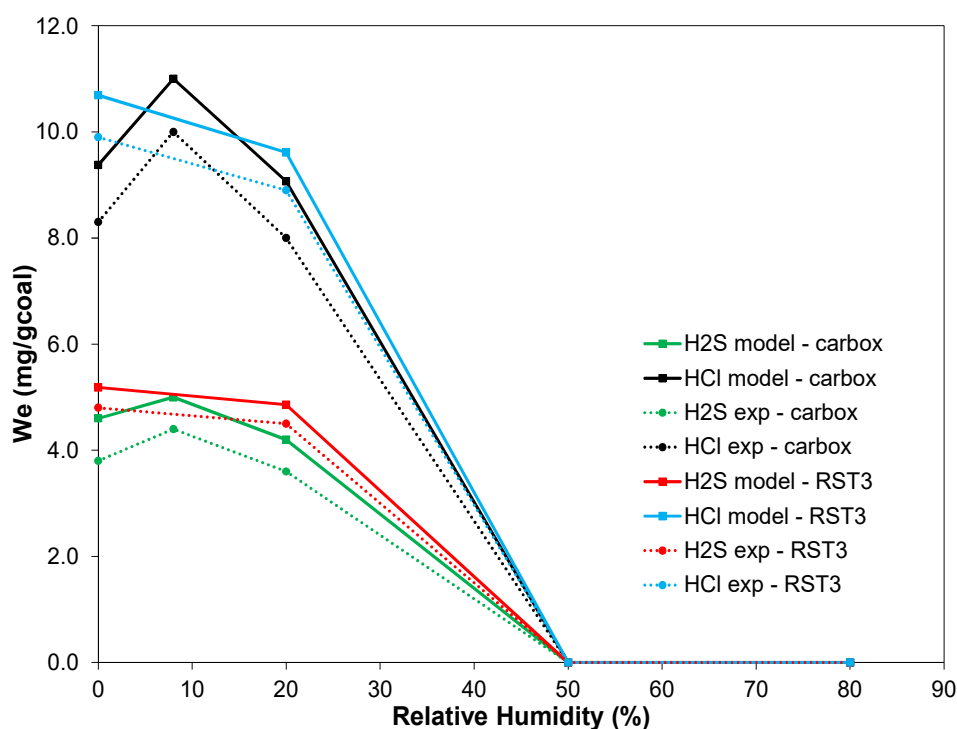
Figure 6 – Adsorption capacity trend versus relative humidity content of biogas

RST3 sample shows a decreasing of the adsorption capacity increasing the relative humidity value, from a maximum value at dry condition, which is experimentally around at 9.9 mg/g and 4.8 mg/g, respectively for HCl and H_2S. Carbox sample shows an increasing of the adsorption capacity value increasing the relative humidity up to 10%. The adsorption capacity decreases from 10 mg/g and 4.4 mg/g, respectively for HCl and H_2S up to zero, considering the relative humidity range from

10% to 50%. Carbox sample shows the best performance with a relative humidity around 10% both for HCl and H_2S pollutant. This is supposed due to the combination of pull-off force and the relative humidity values, considering also the interactions with the metal elements, contained in the Carbox sample instead of RST3 and the microstructure of the carbons [49].
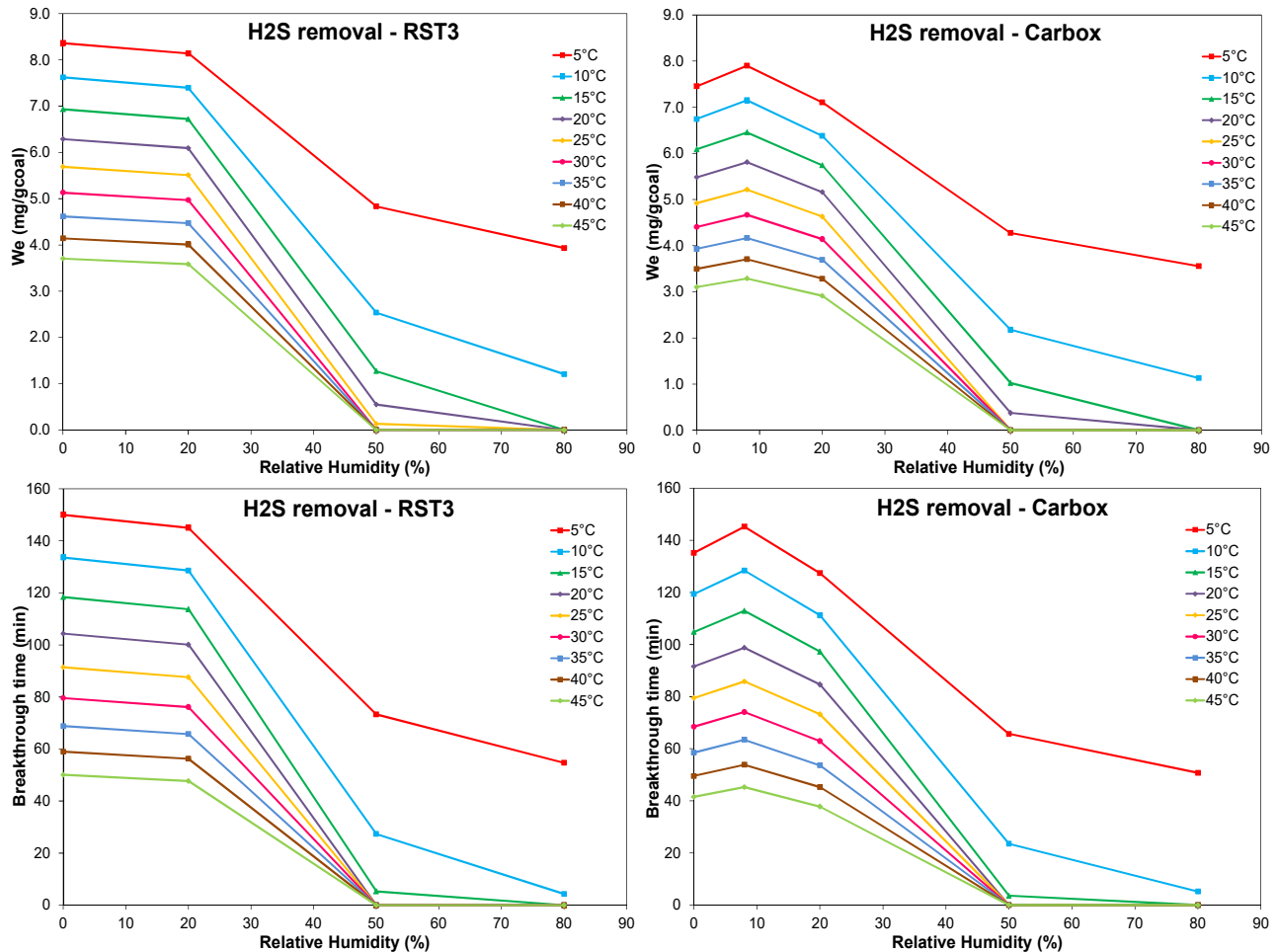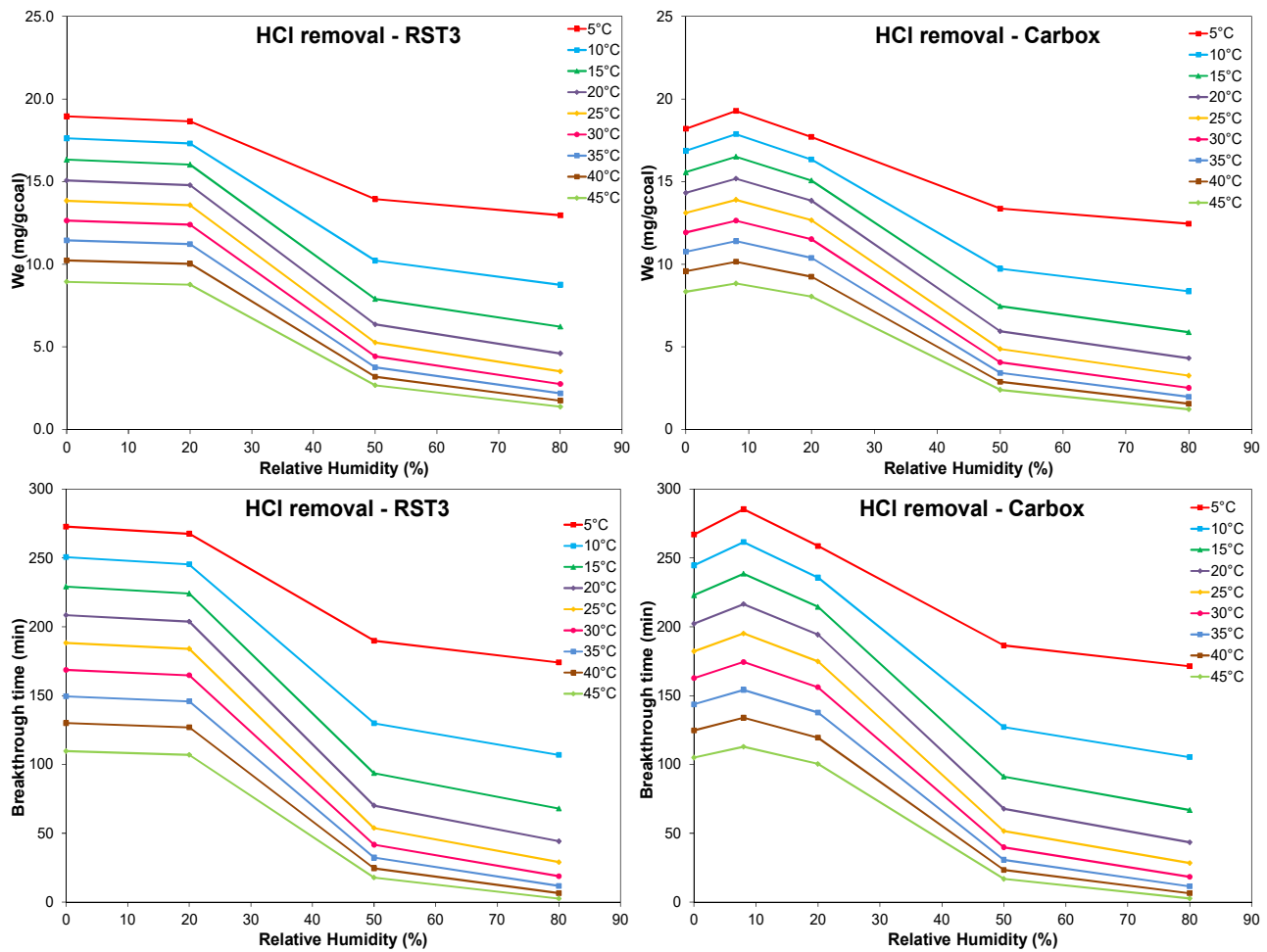

Figure 7 – Breakthrough time and adsorption capacity trend versus relative humidity content of biogas for H_2S

Figure 7 depicts the adsorption capacity and the breakthrough time trend for H_2S varying the relative humidity and the operating temperature. It is highlighted how increasing the operating temperature the adsorption capacity and the breakthrough time show a decreasing rate. For RST3, the adsorption capacity at RH 0% passes from 8.36 mg/g, at 5 °C up to 3.7 mg/g, at 45 °C while above RH 50% and above 25 °C, the adsorption capacity is around zero. The adsorption capacity at RH 80% shows different values to zero for temperature below 15 °C. Hence the adsorption capacity

20

is zero when the operating temperature are above 20 °C. For Carbox sample the adsorption capacity at RH 0% passes from 7.45 mg/g, at 5 °C up to 3.1 mg/g, at 45 °C, while above RH 50% and above 25 °C, the adsorption capacity is around zero. The adsorption capacity at RH 80% shows values different to zero for temperature below 15 °C. Bringing the relative humidity from 0% to 10%, there is an increasing trend on the adsorption capacity that passes from 6.8%, at 5 °C to 6.1%, at 25 °C and 7.7%, at 35 °C. With relative humidity value around 10%, the adsorption capacity shows a decreasing trend more soft compared to RST3. This is true even if for RST3 sample, changing the operating temperature, the absolute value of We was higher.

The breakthrough time shows similar trend to the adsorption capacity (We). Varying the RH value the t_b, at 5 °C and RH 0% is 150 min, while at 45 °C the t_b is around 50 min, for RST3. Considering the same RH condition, the t_b, at 5 °C is 135 min at RH 0%, while at 45 °C the t_b is around 41 min, for Carbox. At relative humidity of 80% the t_b passes from 54.7 min, at 5 °C up to 4.3 min, at 10 °C. While, still for RST3, above 15 °C the t_b is zero. Considering the Carbox sample, at relative humidity of 80% the t_b passes from 50.7 min, at 5 °C up to 5.2 min, at 10 °C, while above 15 °C the t_b is zero.

Figure 8 – Breakthrough time and adsorption capacity trend versus relative humidity content of biogas for HCl

Figure 8 depicts the adsorption capacity and the breakthrough time trend for HCl varying the relative humidity and the operating temperature. Increasing the operating temperature decreases the adsorption capacity. Below 20 °C and above RH 50%, a strong adsorption capacity decrease is recorded. For RST3 the adsorption capacity at RH 0% passes from 18.9 mg/g, at 5 °C up to 8.9 mg/g, at 45 °C. Above RH 50% the adsorption capacity is above zero compared to the removal of H_2S. For Carbox the adsorption capacity at RH 0% passes from 18.2 mg/g, at 5 °C up to 8.3 mg/g, at 45 °C. Here, respect to H_2S removal case, above RH 50% the adsorption capacity is above zero. The adsorption capacity, at RH 80% shows values above 0 mg/g for all the operating temperature considered, both for RST3 and Carbox sample. Considering Carbox sample, bringing the relative humidity from 0% to 10%, there is an increasing trend on the adsorption capacity of 6.0% at 5 °C,

22

6.3% at 20 °C and 18.1% at 45 °C. When relative humidity is 10% the adsorption capacity shows a decreasing trend more soft compared to RST3 case. Even if for RST3 sample, changing the operating temperature, the absolute values of We are higher respect to Carbox sample.

The breakthrough time shows similar trend to We, varying the RH value, the t_b at 5 °C is 273 min at RH 0%, while at 45 °C the t_b is around 110 min, for RST3. Considering the same RH condition, the t_b at 5 °C and RH 0% is 267 min while at 45 °C the t_b is around 105 min, for Carbox. At relative humidity of 80% the t_b passes from 174 min, at 5 °C up to 2.5 min at 45 °C, for RST3. Considering the Carbox sample, at relative humidity of 80% the t_b passes from 171 min, at 5 °C up to 2.6 min at 45 °C. It results that RST3 shows better performance, especially at dry donditions, rexpect to Carbox sample. The Carbox sample shows good performance at RH around 10%.

The HCl removal case shows higher adsorption capacity and breakthrough time values respect to the H2S case. This is due to the higher dipole moment of HCl (1.08 D) compared to H2S (0.95 D) [26][28]. The dipole moment is a measure of degree of polarity. The phenomenon explained as follows: the higher the polarity of compounds of interest is the stronger electron-donating ability become [50].

The combination of the operating temperature and relative humidity on the breakthrough time and on the adsorption capacity, as reported by figure 7 and 8, show an almost inversely proportional behavior. This is due to the slightly exothermal process that, for the operating temperature increases, it will probably enhance chemisorption respect to the physical adsorption [47,48]. Moreover, increasing also the relative humidity, the contemporary presence of water molecules interfere with the removal performance of organic vapors.

Co-vapors influence on the Wheeler-Jonas parameters

In this section are reported the effects of co-vapors, multiple component, on the Wheeler-Jonas parameters. These parameters are breakthrough time, adsorption capacity and adsorption global coefficient. Equations 1-3 and 4-9 must be taken into account to consider the wet state and the multiple contaminant condition. The results are reported in the following tables, 3-4.

Considering RST3 sample, it results that for the t_b value, the discrepancy percentage from model and experimental values range from 22% to 2%, in case of co-vapors and single pollutant case. Considering the adsorption capacity (We) and adsorption global coefficient (kv), the experimental values are estimated indirectly knowing the breakthrough time and their relation. Here the discrepancy from model and experimental values ranges around 8%, for both of them. These discrepancy values are also found for the Carbox sample.

	Starting conc. (ppm(v))	t_b [min]		W_e [mg/g$_{coal}$]		k_v [min^{-1}]	
		Model	Exp.	Model	Exp.	Model	Exp.
H$_2$S + HCl	dry	33	27	7.8	7.2	12051	11087
	wet	31.5	24	7.2	6.6	11818	10873
H$_2$S	dry	61	57	5.4	4.9	9713	9470
	wet	58	54	5	4.5	9581	9302
HCl	dry	103	94	10.6	9.6	14297	13939
	wet	98	91	10.1	8.9	14051	13642

Table 4 – co-vapors effect on Wheeler-Jonas parameters – RST3

	Starting conc. (ppm(v))	t_b [min]		W_e [mg/g$_{coal}$]		k_v [min^{-1}]	
		Model	Exp.	Model	Exp.	Model	Exp.
H$_2$S + HCl	dry	30	25	7	6.4	10677	9823
	wet	28	21	6.3	5.8	10299	9476
H$_2$S	dry	61	57	5.4	4.9	9713	9470
	wet	49	46	4.2	3.9	8140	7903
HCl	dry	103	94	10.6	9.6	14297	13939
	wet	95	88	9.2	8.4	13010	12631

Table 5 – co-vapors effect on Wheeler-Jonas parameters – Carbox

Taking in consideration the single pollutant case, H_2S for example, to remove 9.6 ppm(v) in dry condition for RST3, the breakthrough time required is about 61 min while it decreases of almost 45.9% to 33 min, with the contemporary presence of HCl and 45.7%, in wet condition. Single HCl removal test shows a more strong removal performance decrease with multiple contaminants. The breakthrough time to remove only HCl for RST3, in dry condition, is around 103 min and it decreases to 33 min considering the contemporary presence of also H_2S. The wet condition worsens even more the removal performance. The removal performance are similar considering the Carbox sample. Here, the decreasing rate of performance worsens in dry condition but improves in wet condition. Considering the t_b, the removal performance for H_2S, with multiple contaminant and dry condition decreases of 50.8% against 45.9% with RST3. In wet condition the t_b decreases of 42.9% against 45.7% with RST3. These results show how Carbox is better in wet condition with a RH value around 20%. For the removal of HCl, the performance trend is similar to RST3: the decreasing rate is 70.9% and 70.5% in dry and wet state, respectively. In this case, for the wet condition value (20%), does not help the removal performance of HCl as it was instead demonstrated by the H_2S case. For the adsorption capacity and the adsorption global coefficient, similar but opposite trends are reported for H_2S and HCl. Here, for H_2S the adsorption capacity increases of 44% for RST3, wet and dry condition while it increases of 30% and 50% for Carbox, dry and wet condition. Considering HCl, again both dry and wet state, show a similar behavior with a decreasing of the adsorption capacity in the multiple contaminant case. This is due to the fact that H_2S is easily adsorbed on the carbon material respect to HCl. H_2S undermines HCl and for this reason increases its adsorption capacity, while the behavior for the HCl removal decreases. A similar behavior is reported for the adsorption global coefficient.

4. **Conclusions**

The Wheeler-Jonas parameters for biogas trace compounds removal were evaluated considering several operating variables: different sorbent material, gas condition (dry or wet), temperature and considering the multiple contaminant state (H_2S+HCl). Results showed how two similar commercial activated carbons display different behavior. RST3 sample in dry condition shows better removal performance than Carbox at same operating temperature and for the same pollutant removal species. Considering the wet condition, Carbox sample improves its removal performance up to working optimally around 10-20% of relative humidity. Here, Carbox shows better removal performance for H_2S and HCl, respect to RST3. Increasing the operating temperature the removal performance generally worse. This is due to the slightly exothermal process that will probably enhance chemisorption but has disadvantage on the physical adsorption. Finally, the multiple contaminants condition in dry and wet condition was studied and modeled. The model adopted showed results reliable with a discrepancy value around 8%. Here, results showed a general decrease on the removal performance for both sorbent materials adopted and gas conditions. For H_2S removal and for wet condition, this decreasing trend is softer considering the Carbox sample, respect to RST3. Future works will focus on the t_b estimation of more than a binary mixture (H_2S+HCl), estimating the service life time of a clean-up system for SOFC applications fed by biogas.

Acknowledgements

References

[1]   L.M.A. Bettencourt, J.E. Trancik, J. Kaur, Determinants of the Pace of Global Innovation in Energy Technologies, PLoS One. 8 (2013) 1–6. doi:10.1371/journal.pone.0067864.

[2]   L.K. K. Takahashi, S. Baker, Policy Options to Support Distributed Resources, Delaware, 2005.

[3]   N.T. Raj, S. Iniyan, R. Goic, A review of renewable energy based cogeneration technologies, Renew. Sustain. Energy Rev. 15 (2011) 3640–3648. doi:10.1016/j.rser.2011.06.003.

[4]   C. Song, Fuel processing for low-temperature and high-temperature fuel cells: Challenges, and opportunities for sustainable development in the 21st century, Catal. Today. 77 (2002) 17–49. doi:10.1016/S0920-5861(02)00231-6.

[5]   M. Lo Faro, V. Antonucci, P.L. Antonucci, A.S. Aricó, Fuel flexibility: A key challenge for SOFC technology, Fuel. 102 (2012) 554–559. doi:10.1016/j.fuel.2012.07.031.

[6]   D. Papurello, A. Lanzini, L. Tognana, S. Silvestri, M. Santarelli, Waste to energy: Exploitation of biogas from organic waste in a 500 Wel solid oxide fuel cell (SOFC) stack, Energy. 85 (2015) 145–158. doi:10.1016/j.energy.2015.03.093.

[7]   J. Van Herle, Y. Membrez, O. Bucheli, Biogas as a fuel source for SOFC co-generators, J. Power Sources. 127 (2004) 300–312. doi:10.1016/j.jpowsour.2003.09.027.

[8]   J. Staniforth, K. Kendall, Biogas powering a small tubular solid oxide fuel cell, J. Power Sources. 71 (1998) 275–277. doi:10.1016/S0378-7753(97)02762-6.

[9]   A.A. Trendewicz, R.J. Braun, Techno-economic analysis of solid oxide fuel cell-based combined heat and power systems for biogas utilization at wastewater treatment facilities, J. Power Sources. 233 (2013) 380–393. doi:10.1016/j.jpowsour.2013.01.017.

[10]   S. Wongchanapai, H. Iwai, M. Saito, H. Yoshida, Performance evaluation of a direct-biogas solid oxide fuel cell-micro gas turbine (SOFC-MGT) hybrid combined heat and power (CHP) system, J. Power Sources. 223 (2013) 9–17. doi:10.1016/j.jpowsour.2012.09.037.

[11]   D. Papurello, C. Soukoulis, E. Schuhfried, L. Cappellin, F. Gasperi, S. Silvestri, et al., Monitoring of volatile compound emissions during dry anaerobic digestion of the Organic Fraction of Municipal Solid Waste by Proton Transfer Reaction Time-of-Flight Mass Spectrometry, Bioresour. Technol. 126 (2012) 254–265. doi:10.1016/j.biortech.2012.09.033.

[12]   K. Sasaki, K. Haga, T. Yoshizumi, D. Minematsu, E. Yuki, R. Liu, et al., Chemical durability of Solid Oxide Fuel Cells: Influence of impurities on long-term performance, J. Power Sources. 196 (2011) 9130–9140. doi:10.1016/j.jpowsour.2010.09.122.

[13] D. Papurello, R. Borchiellini, P. Bareschino, V. Chiodo, S. Freni, A. Lanzini, et al., Performance of a Solid Oxide Fuel Cell short-stack with biogas feeding, Appl. Energy. 125 (2014) 254–263.

[14] D. Papurello, A. Lanzini, P. Leone, M. Santarelli, S. Silvestri, Biogas from the organic fraction of municipal solid waste: Dealing with contaminants for a solid oxide fuel cell energy generator, Waste Manag. (2014).

[15] A. Hagen, J.F.B. Rasmussen, K. Thydén, Durability of solid oxide fuel cells using sulfur containing fuels, J. Power Sources. 196 (2011) 7271–7276. doi:10.1016/j.jpowsour.2011.02.053.

[16] J.F.B. Rasmussen, A. Hagen, The effect of H2S on the performance of Ni-YSZ anodes in solid oxide fuel cells, J. Power Sources. 191 (2009) 534–541. doi:10.1016/j.jpowsour.2009.02.001.

[17] D. Papurello, A. Lanzini, S. Fiorilli, F. Smeacetto, R. Singh, M. Santarelli, Sulfur poisoning in Ni-anode solid oxide fuel cells (SOFCs): Deactivation in single cells and a stack, Chem. Eng. J. 283 (2016) 1224–1233. doi:10.1016/j.cej.2015.08.091.

[18] N. de Arespacochaga, C. Valderrama, C. Mesa, L. Bouchy, J.L. Cortina, Biogas deep clean-up based on adsorption technologies for Solid Oxide Fuel Cell applications, Chem. Eng. J. 255 (2014) 593–603. doi:10.1016/j.cej.2014.06.072.

[19] Z. Shareenfdeen, B. Herner, D. Webb, S. Wilson, Biofiltration eliminates nuisance chemical odors from industrial air streams, J. Ind. Microbiol. Biotechnol. 30 (2003) 168–174.

[20] D. Ramírez-Sáenz, P.B. Zarate-Segura, C. Guerrero-Barajas, E.I. García-Peña, H2S and volatile fatty acids elimination by biofiltration: Clean-up process for biogas potential use, J. Hazard. Mater. 163 (2009) 1272–1281. doi:10.1016/j.jhazmat.2008.07.129.

[21] N. Abatzoglou, S. Boivin, A review of biogas purification processes, Biofuels, Bioprod. Biorefining. 6 (2009) 42–71. doi:10.1002/bbb.

[22] S.P. Hernández, F. Scarpa, D. Fino, R. Conti, Biogas purification for MCFC application, Int. J. Hydrogen Energy. 36 (2011) 8112–8118. doi:10.1016/j.ijhydene.2011.01.055.

[23] D. Papurello, L. Tomasi, S. Silvestri, I. Belcari, M. Santarelli, F. Smeacetto, et al., Biogas trace compound removal with ashes using proton transfer reaction time-of-flight mass spectrometry as innovative detection tool, Fuel Process. Technol. 145 (2016) 62–75. doi:10.1016/j.fuproc.2016.01.028.

[24] W. Yuan, T.J. Bandosz, Removal of hydrogen sulfide from biogas on sludge-derived adsorbents, Fuel. 86 (2007) 2736–2746. doi:10.1016/j.fuel.2007.03.012.

[25] R.T. Yang, Gas Separation by Adsorption Processes, Butterworths, 1988. doi:10.1016/0950-4214(88)80042-2.

[26] M.L. McGlashan, National Physical Laboratory, Tables of Physical and chemical constants – dipole moments, (n.d.). http://www.kayelaby.npl.co.uk/chemistry/3_7/3_7_1.html.

[27] M. Simao, E. Carvalho Filho, The Dipole Moments of Alkanethiols, 62 (1958) 1427–1430.

[28] M. Blaber, Dipole Moments, (n.d.). http://chemwiki.ucdavis.edu/Physical_Chemistry/Atomic_Theory/Dipole_Moments (accessed January 21, 2015).

[29] D. Papurello, E. Schuhfried, A. Lanzini, A. Romano, L. Cappellin, T.D. Märk, et al., Proton transfer reaction-mass spectrometry as a rapid inline tool for filter efficiency of activated charcoal in support of the development of Solid Oxide Fuel Cells fueled with biogas, Fuel Process. Technol. 130 (2015) 78–86. doi:10.1016/j.fuproc.2014.09.042.

[30] D. Papurello, E. Schuhfried, A. Lanzini, A. Romano, L. Cappellin, T.D. Märk, et al., Influence of co-vapors on biogas filtration for fuel cells monitored with PTR-MS (Proton Transfer Reaction-Mass Spectrometry), Fuel Process. Technol. 118 (2014) 133–140. doi:10.1016/j.fuproc.2013.08.011.

[31] P. Lodewyckx, G.O. Wood, S.K. Ryu, The Wheeler-Jonas equation: A versatile tool for the prediction of carbon bed breakthrough times, Carbon N. Y. 42 (2004) 1345–1349. doi:10.1016/j.carbon.2004.01.016.

[32] P. Lodewyckx, L. Verhoeven, Using the modified Wheeler-Jonas equation to describe the adsorption of inorganic molecules: Chlorine, Carbon N. Y. 41 (2003) 1215–1219. doi:10.1016/S0008-6223(03)00052-6.

[33] P. Lodewyckx, L. Verhoeven, Using the Wheeler-Jonas equation to describe adsorption of inorganic molecules: ammonia, Carbon N. Y. 41 (2003) 1215–1219. doi:10.1016/S0008-6223(03)00052-6.

[34] G.O. Wood, P. Lodewyckx, Correlations for high umidity corrections of rate coefficients for adsorption of organic vapors and gases on activated carbons in air-purifying respirator cartridges, J. Int. Soc. Respir. Prot. (2002) 58–64.

[35] P. Lodewyckx, E.F. Vansant, Prediction of Breakthrough Times of Water Immiscible Organic Vapors on Activated Carbon Beds, Am. Ind. Hyg. Assoc. J. 60 (2010) 612–617.

doi:10.1080/00028899908984480.

[36]   G.O. Wood, Activated carbon adsorption capacities for vapors, Carbon N. Y. 30 (1992) 593–599.

[37]   O. Busmundrud, Vapour breakthrough in activated carbon beds, Carbon N. Y. 31 (1993).

[38]   L.A. Jonas, The rate of gas adsorption by activated carbon, Carbon N. Y. 12 (1974).

[39]   GO. Wood, Activated carbon adsorption capacities for vapors, Carbon N. Y. 30 (1992) 593.

[40]   J.F. Stampfer, G.O. Wood, Adsorption rate coefficients for gases and vapors on activated carbons, Carbon N. Y. 31 (1993) 195.

[41]   G.O. Wood, P. Lodewyckx, An extended equation for rate coefficients for adsorption of organic vapors and gases on activated carbons in air-purifying respirator cartridges, Am Ind Hyg Assoc J. 64 (2003) 646.

[42]   P. Lodewyckx, Estimating the overall mass transfer coefficient kv of the Wheeler–Jonas equation: a new and simple model, Am Ind Hyg Assoc J. 61 (2000) 501–506.

[43]   R.C. Reid, J.M. Prausnitz, B.E. Poling, The Properties of Gases & Liquids, 4th Edition, 4th ed., McGraw-Hill, inc., New York, 1987.

[44]   P. Lodewyckx, E.F. Vansant, The Influence of Humidity on the Overall Mass Transfer Coefficient of the Wheeler-Jonas Equation, AIHAJ - Am. Ind. Hyg. Assoc. 61 (2000) 461–468. doi:10.1080/15298660008984556.

[45]   P. Lodewyckx, E.F. Vansant, Influence of Humidity on Adsorption Capacity from the Wheeler-Jonas Model for Prediction of Breakthrough Times of Water Immiscible Organic Vapors on Activated Carbon Beds, Am. Ind. Hyg. Assoc. J. 60 (1999) 612–617. doi:10.1080/00028899908984480.

[46]   H.S. Choo, L.C. Lau, A.R. Mohamed, K.T. Lee, Hydrogen sulfide adsorption by alkaline impregnated coconut shell activated carbon, J. Eng. Sci. Technol. 8 (2013) 741–753.

[47]   Y. Xiao, S. Wang, D. Wu, Q. Yuan, Experimental and simulation study of hydrogen sulfide adsorption on impregnated activated carbon under anaerobic conditions, J. Hazard. Mater. 153 (2008) 1193–1200. doi:10.1016/j.jhazmat.2007.09.081.

[48]   M.J. Lashaki, M. Fayaz, H. Wang, Z. Hashisho, J.H. Philips, J.E. Anderson, et al., Effect of adsorption and regeneration temperature on irreversible adsorption of organic vapors on

beaded activated carbon, Environ. Sci. Technol. 46 (2012) 4083–4090. doi:10.1021/es3000195.

[49] R.J.W. T. Thundat, X.Y. Zheng, G.Y. Chen, Role of relative humidity in atomic force microscopy imaging., Surf. Sci. Lett. 294 (1993) L939–L43.

[50] X. Yang, J. Li, T. Wen, X. Ren, Y. Huang, X. Wang, Colloids and Surfaces A : Physicochemical and Engineering Aspects Adsorption of naphthalene and its derivatives on magnetic graphene composites and the mechanism investigation, Colloids Surfaces A Physicochem. Eng. Asp. 422 (2013) 118–125. doi:10.1016/j.colsurfa.2012.11.063.

Table captions

Table 1 – Dipole moment for VOCs of interest

Table 2 – Commercial activated carbons characteristics

Table 3 – Elements identified with SEM-EDS analysis in the Carbox and RST3 sample.

Table 4 – co-vapors effect on Wheeler-Jonas parameters – RST3

Table 5 – co-vapors effect on Wheeler-Jonas parameters – Carbox

Table 1

Compound	Dipole moment (Debye)	Reference
Hydrogen sulfide	0.95	[26]
Methanethiol	1.52	[26]
Dimetylsulfide	1.58	[26]
Propanethiol	1.55	[27]
Butanethiol	1.54	[27]
Chloroethane	6.7	[26]
2-Butanone	2.76	[26]
Toluene	1.3	[26]
Styrene	0.3	[26]
HF	1.82	[28]
HCl	1.08	[28]
HBr	0.82	[28]
HI	0.44	[28]

Table 2

Sample	Specific Surface Area (m^2/g)	V total (cm^3/g)	V microporous (cm^3/g)
Airdep Carbox	1237	0.407	0.328
RST3	1117	0.447	0.300

Table 3

Atomic %	Virgin		Tested	
Element	Carbox	RST3	Carbox	RST3
C	80.9	91.15	86.96	93.83
O	9.01	5.3	8.37	4.6
Mg	1.19	0.2	0.1	0.08
Al	1.98		0.68	
Si	1.4		1.03	
P	0.81			
S	0.11	0.57	0.27	0.72
Cl	0.33		0.63	
K	0.78	0.78	0.21	0.37
Ca	1.65	0.76	1.03	0.4
Mn	0.41			
Fe	1.43		0.72	
Zn		1.15		
Total:	100	100	100	100

Table 4

	Starting conc. (ppm(v))	t_b [min]		W_e [mg/g$_{coal}$]		k_V [min^{-1}]	
		Model	Exp.	Model	Exp.	Model	Exp.
H$_2$S + HCl	dry	33	27	7.8	7.2	12051	11087
	wet	31.5	24	7.2	6.6	11818	10873
H$_2$S	dry	61	57	5.4	4.9	9713	9470
	wet	58	54	5	4.5	9581	9302
HCl	dry	103	94	10.6	9.6	14297	13939
	wet	98	91	10.1	8.9	14051	13642

Table 5

	Starting conc. (ppm(v))	t_b [min]		W_e [mg/g_{coal}]		k_V [min^{-1}]	
		Model	Exp.	Model	Exp.	Model	Exp.
H₂S + HCl	dry	30	25	7	6.4	10677	9823
	wet	28	21	6.3	5.8	10299	9476
H₂S	dry	61	57	5.4	4.9	9713	9470
	wet	49	46	4.2	3.9	8140	7903
HCl	dry	103	94	10.6	9.6	14297	13939
	wet	95	88	9.2	8.4	13010	12631

Figure captions

Figure 1 – Experimental set-up

Figure 2 – Breakthrough time trend versus initial concentration of the pollutant

Figure 3 – Adsorption capacity trend versus initial concentration of the pollutant

Figure 4 – Breakthrough time trend versus operating temperature

Figure 5 – Adsorption capacity trend versus operating temperature

Figure 6 – Adsorption capacity trend versus relative humidity content of biogas

Figure 7 – Breakthrough time and adsorption capacity trend versus relative humidity content of biogas for H_2S

Figure 8 – Breakthrough time and adsorption capacity trend versus relative humidity content of biogas for HCl
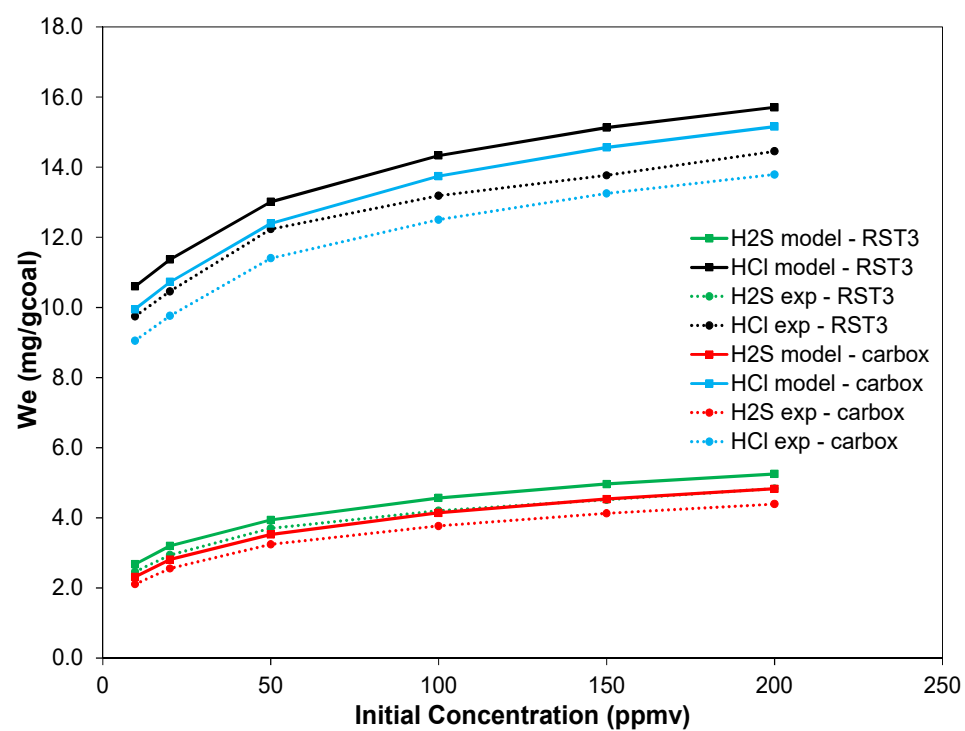
Figure 1

Mass spectrometer

Heated trap

Blank line

Biogas (CH₄/ CO₂) + H₂S/HCl + H₂O

PDMS filter

AC filter
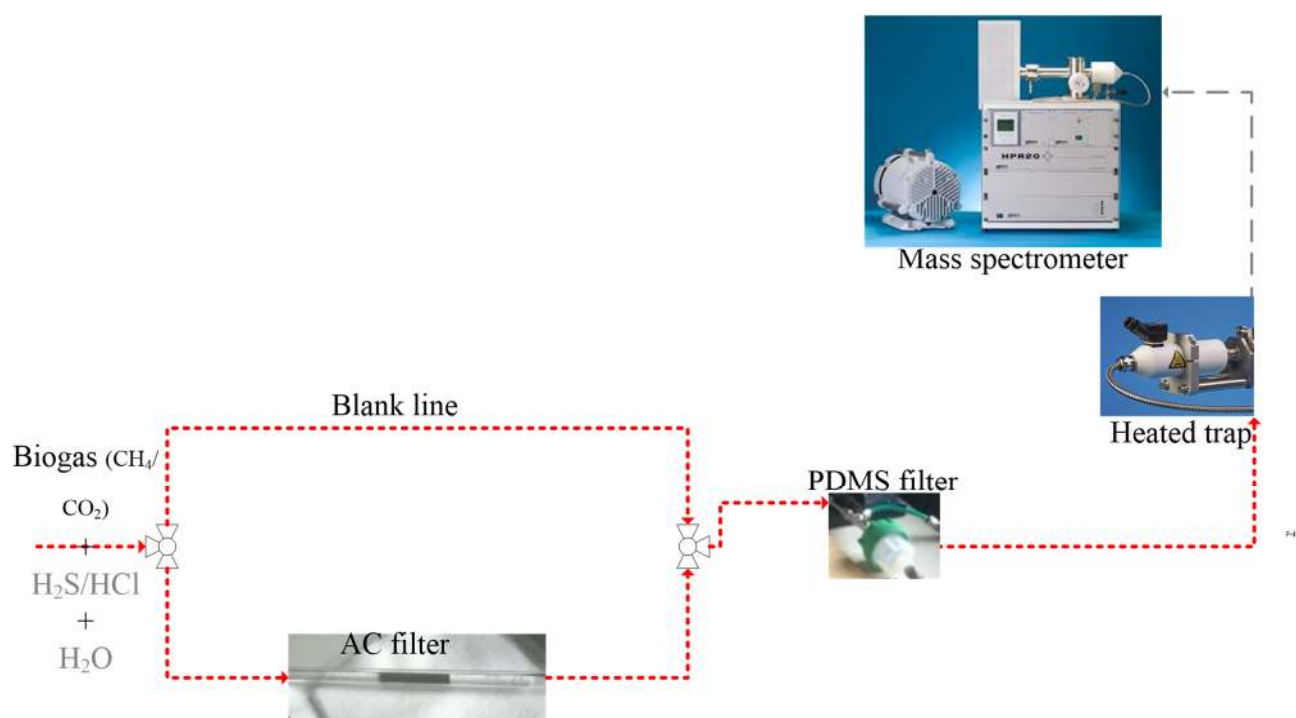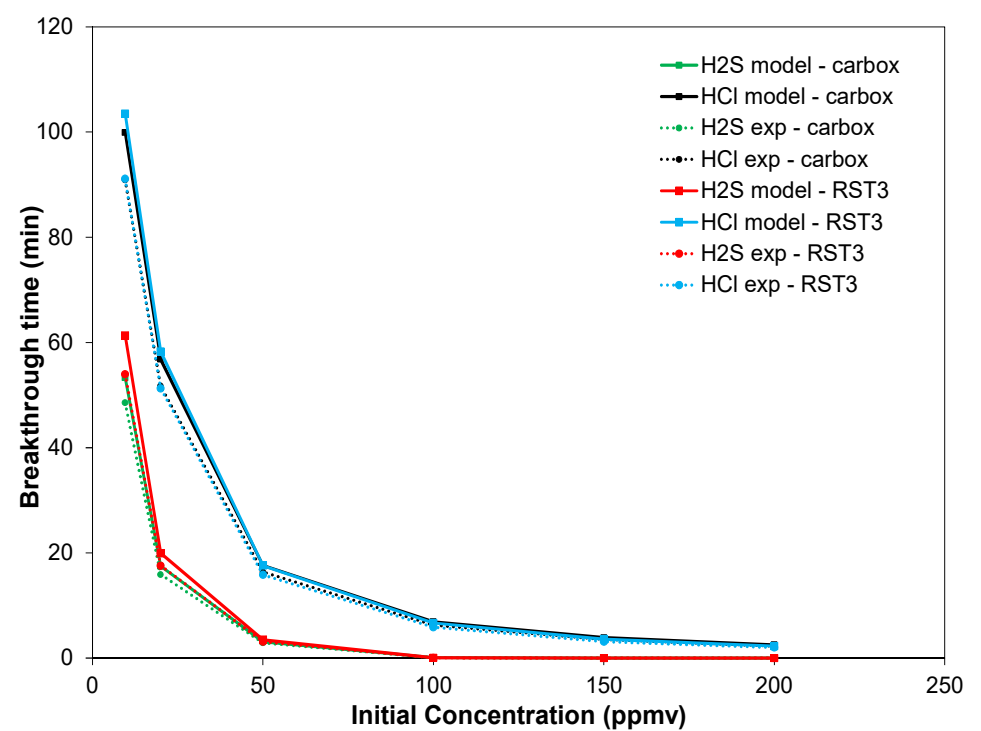
Figure 2

Figure 3

Figure 4
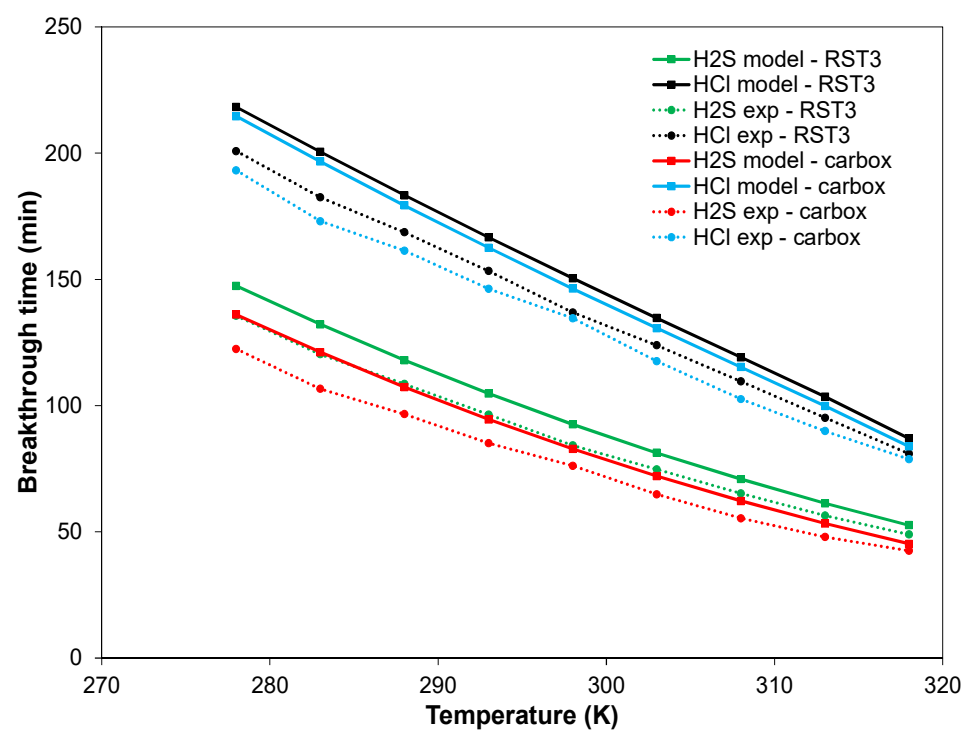
Figure 5
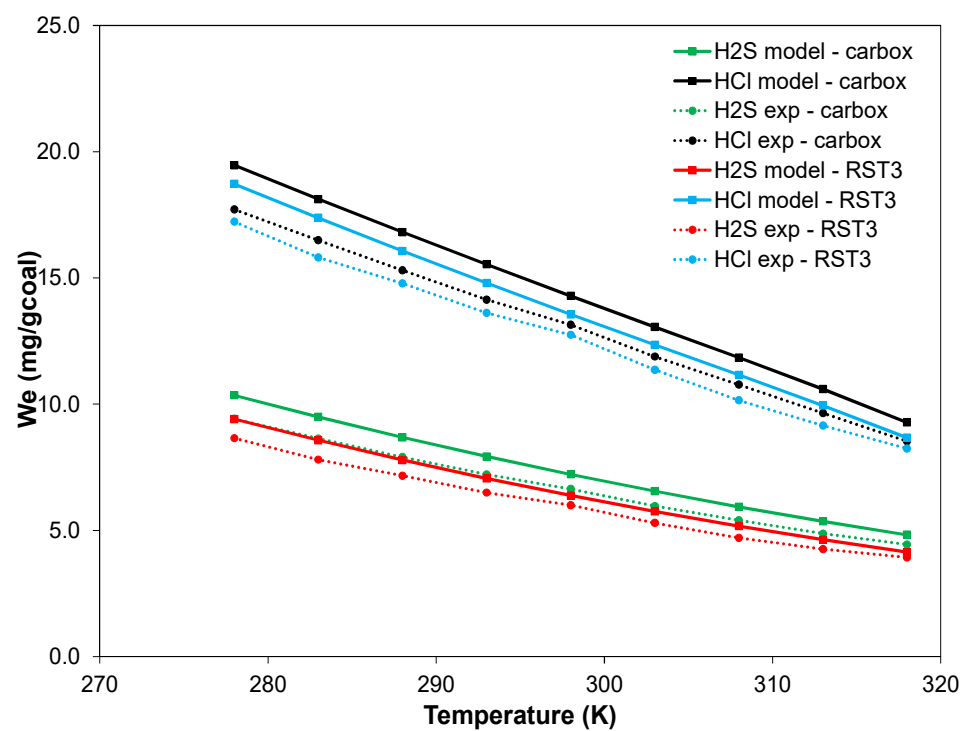
Figure 6

Figure 7

Figure 8